
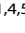


## ARTICLE OPEN



# USP30 inhibition induces mitophagy and reduces oxidative stress in parkin-deficient human neurons

Justyna Okarmus<sup>1</sup>, Jette Bach Agergaard<sup>1</sup>, Tina C. Stummann<sup>2</sup>, Henriette Haukedal<sup>3</sup>, Malene Ambjørn<sup>2</sup>, Kristine K. Freude<sup>3</sup>, Karina Fog<sup>2</sup> and Morten Meyer<sup>1,4,5</sup>  

© The Author(s) 2024

Ubiquitination of mitochondrial proteins plays an important role in the cellular regulation of mitophagy. The E3 ubiquitin ligase parkin (encoded by *PARK2*) and the ubiquitin-specific protease 30 (USP30) have both been reported to regulate the ubiquitination of outer mitochondrial proteins and thereby mitophagy. Loss of E3 ligase activity is thought to be pathogenic in both sporadic and inherited Parkinson's disease (PD), with loss-of-function mutations in *PARK2* being the most frequent cause of autosomal recessive PD. The aim of the present study was to evaluate whether mitophagy induced by USP30 inhibition provides a functional rescue in isogenic human induced pluripotent stem cell-derived dopaminergic neurons with and without *PARK2* knockout (KO). Our data show that healthy neurons responded to CCCP-induced mitochondrial damage by clearing the impaired mitochondria and that this process was accelerated by USP30 inhibition. Parkin-deficient neurons showed an impaired mitophagic response to the CCCP challenge, although mitochondrial ubiquitination was enhanced. USP30 inhibition promoted mitophagy in *PARK2* KO neurons, independently of whether left in basal conditions or treated with CCCP. In *PARK2* KO, as in control neurons, USP30 inhibition balanced oxidative stress levels by reducing excessive production of reactive oxygen species. Interestingly, non-dopaminergic neurons were the main driver of the beneficial effects of USP30 inhibition. Our findings demonstrate that USP30 inhibition is a promising approach to boost mitophagy and improve cellular health, also in parkin-deficient cells, and support the potential relevance of USP30 inhibitors as a novel therapeutic approach in diseases with a need to combat neuronal stress mediated by impaired mitochondria.

*Cell Death and Disease* (2024)15:52; <https://doi.org/10.1038/s41419-024-06439-6>

## INTRODUCTION

Parkinson's disease (PD) is a neurodegenerative movement disorder characterized by the progressive loss of mainly midbrain dopaminergic neurons [1]. Despite years of research, there is no cure for PD. Current treatments are symptomatic only and based on dopaminergic drugs that are associated with dyskinesia and reduced effect as the disease progresses [2–4]. The development of alternative PD treatment strategies is therefore of high interest.

The most frequent cause of autosomal recessive PD is loss-of-function mutations in the *PARK2* gene, which encodes for the protein parkin [5]. Parkin inactivation has also been suggested to be implicated in sporadic PD [6, 7]. Investigations of cellular effects of mutations in the *PARK2* gene may therefore reveal common disease mechanisms important for unraveling the pathogenesis of both familial and sporadic PD and thereby guide the identification of novel therapeutic strategies.

Parkin is a key player in the regulation of mitophagy, a fundamental process critical to maintaining mitochondrial health [8]. Loss of the mitochondrial membrane electrochemical

potential leads to dysfunctional oxidative phosphorylation. The membrane depolarization is followed by the stabilization of phosphatase and tensin homolog-induced kinase 1 (PINK1) at the mitochondria membrane, where it phosphorylates ubiquitin and parkin at their respective serine 65 (S65) residues. This recruits parkin to the mitochondria and activates the ubiquitination of many outer mitochondrial membrane proteins. A high total ubiquitination load is the signal for the engulfment of the mitochondria by the autophagosome [9–11]. Mitophagy protects against the accumulation of damaged mitochondria and toxic reactive oxygen species (ROS) [12] and is therefore expected to be neuroprotective [13].

Ubiquitination and deubiquitination are enzymatically mediated processes by which ubiquitin is covalently bound or cleaved from proteins by E3 ubiquitin ligases or deubiquitinating enzymes, respectively [14, 15]. USP30, a deubiquitinase, has been reported to counteract parkin-dependent mitophagy by deubiquitinating outer mitochondrial membrane proteins, in particular TOM20 [13, 16–19]. Knockdown (KD) of USP30 in parkin-

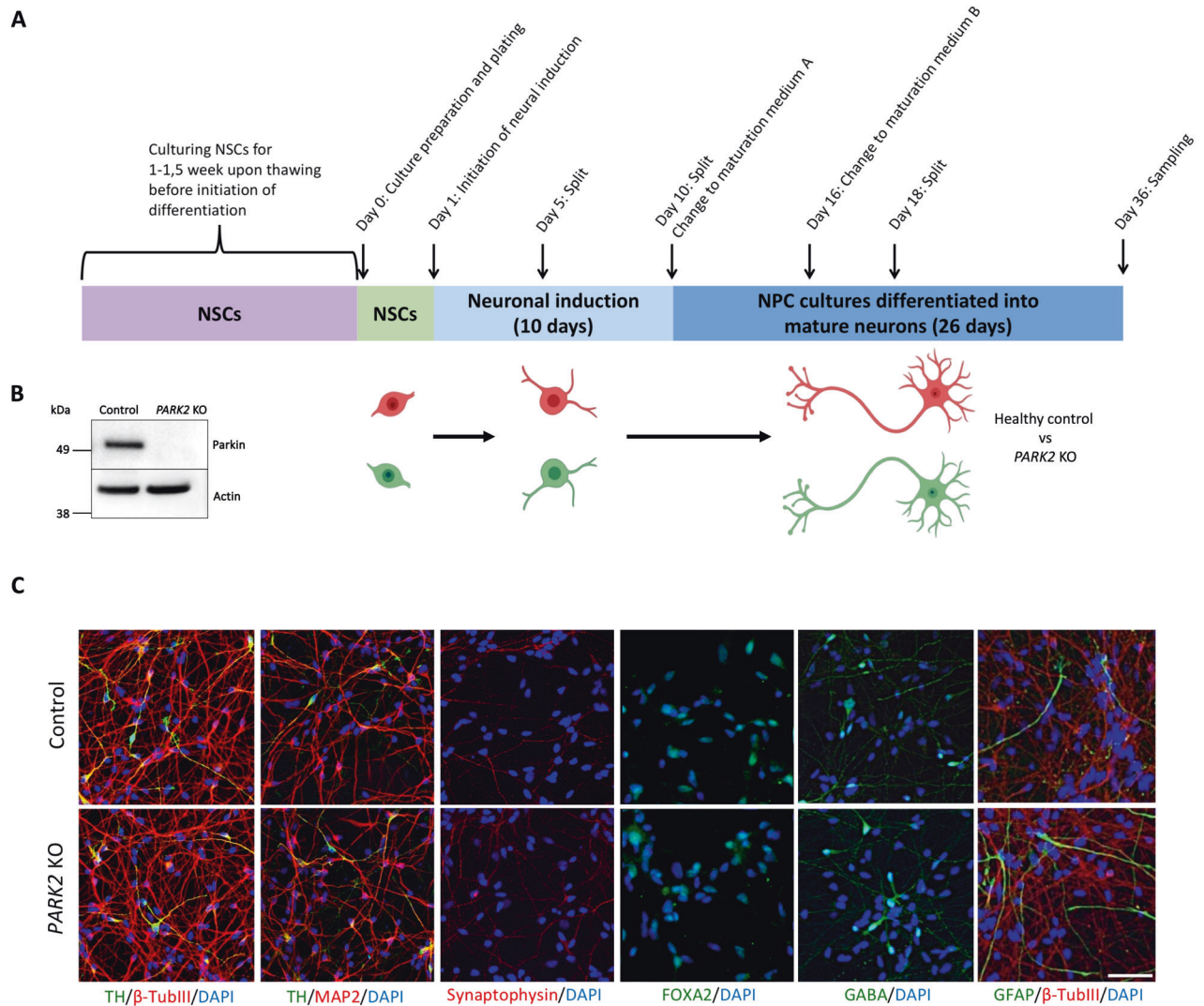
<sup>1</sup>Department of Neurobiology Research, Institute of Molecular Medicine, University of Southern Denmark, J.B. Winsløvs Vej 21, 5000 Odense C, Denmark. <sup>2</sup>Neuroscience, H. Lundbeck A/S, Othilievej 9, 2500 Valby, Denmark. <sup>3</sup>Department of Veterinary and Animal Sciences, Faculty of Health and Medical Sciences, University of Copenhagen, Grønnegaardsvej 7, 1870 Frederiksberg C, Denmark. <sup>4</sup>Department of Neurology, Odense University Hospital, J.B. Winsløvs Vej 4, 5000 Odense C, Denmark. <sup>5</sup>BRIDGE—Brain Research Inter-Disciplinary Guided Excellence, Department of Clinical Research, University of Southern Denmark, J.B. Winsløvs Vej 19, 5000 Odense C, Denmark.

<sup>✉</sup>email: mmeyer@health.sdu.dk

Edited by Professor Pier Giorgio Mastroberardino

Received: 8 December 2022 Revised: 22 December 2023 Accepted: 4 January 2024

Published online: 15 January 2024



**Fig. 1** Derivation and characterization of healthy and *PARK2* KO neurons. **A** Graphical overview of the differentiation of isogenic iPSC-derived neural stem cells (NSCs) into fully committed mature neurons. **B** Western blotting for parkin validating *PARK2* KO. Full-length blot is presented in Supplementary Materials. **C** Immunofluorescence staining of control and *PARK2* KO NSCs differentiated into mature cells showed a large proportion of beta-TubulinIII+ newly formed neurons (red), MAP2+ mature neurons (red), including a significant population of tyrosine hydroxylase (TH)+ dopaminergic neurons (green). The cells also expressed synaptophysin (red, a marker of presynaptic regions) and FOXA2 (green, a marker of the midbrain phenotype). A small population of GABA+ neurons and GFAP+ astrocytes was also present in the cultures. Cell nuclei were stained with DAPI (blue). Scale bar = 50  $\mu$ m.

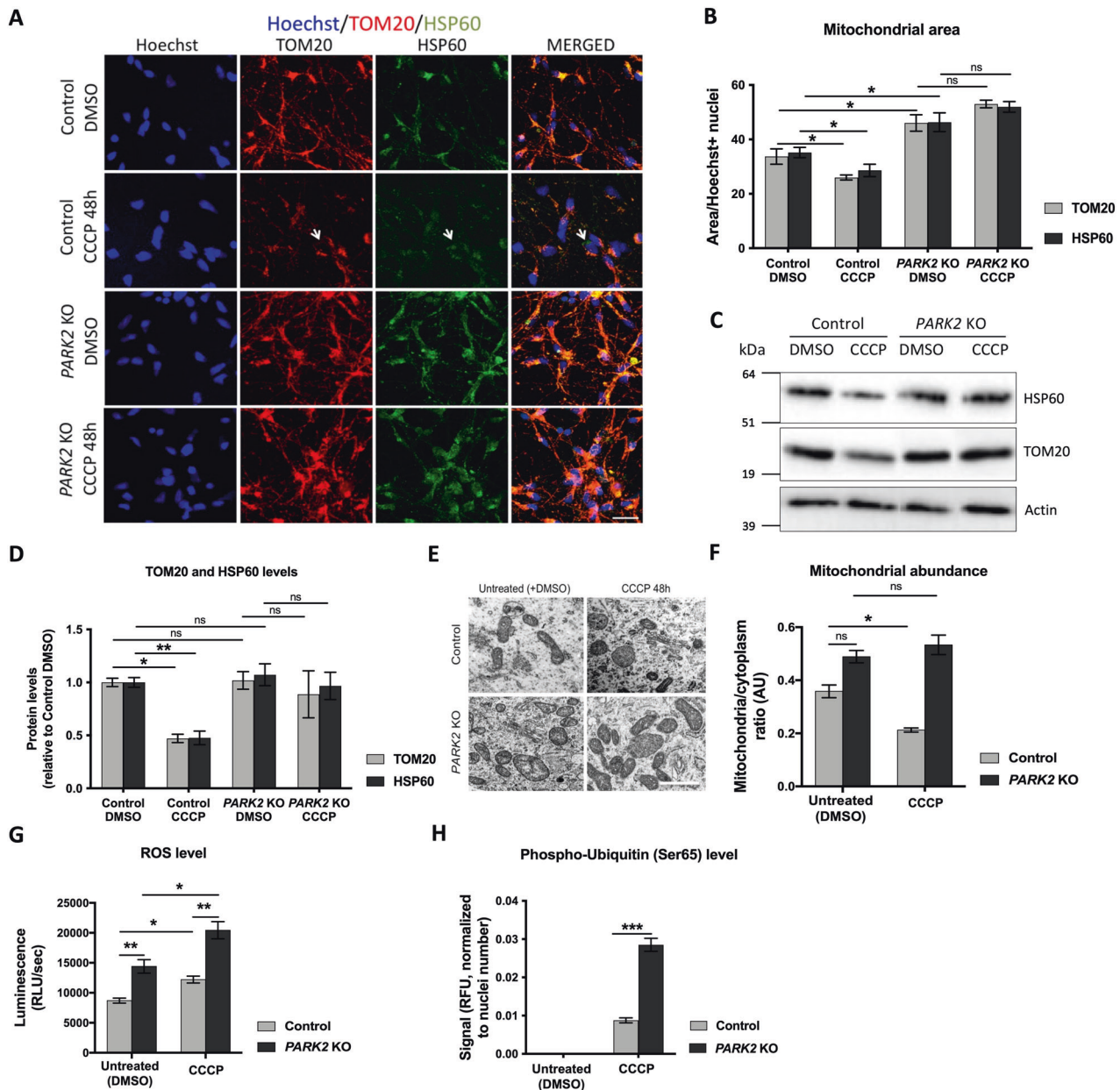
overexpressing cells promotes the clearance of mitochondria in response to mitochondrial depolarizing agents [19]. This suggests that USP30 inhibition may be a therapeutic approach to facilitate mitophagy of dysfunctional mitochondria and rescue neurons.

USP30 KD or inhibition can induce mitophagy in cultured cells [13, 17, 18, 20, 21]. USP30 inhibition was recently shown to increase cardiac mitophagy in vivo [21]. Less is known about the relevance of USP30 in controlling mitophagy induction in the human brain, and specifically in the brains of *PARK2* mutation carriers. Induced pluripotent stem cells (iPSCs) allow for differentiation into human midbrain dopaminergic neurons [22, 23]. In this study, we took advantage of the iPSC technology to generate isogenic human dopaminergic neurons with and without *PARK2* knockout (KO). This enabled us to study the effect of *PARK2* KO on the induction of mitophagy upon chemical mitochondrial damage and the potential of USP30 inhibition to boost mitophagy and decrease oxidative stress in neurons with and without functional parkin protein.

## RESULTS

### Isogenic *PARK2* KO and control cultures contain similar cell populations

To study the disease mechanisms underlining *PARK2*-mediated PD, we compared healthy human iPSCs and isogenic iPSCs where the *PARK2* gene was deleted using zinc finger nuclease gene editing [24]. Detailed information on this cell line can be found in our recent studies [25–28]. Isogenic *PARK2* KO and control iPSC-derived neural stem cells (NSCs) were differentiated into neuronal cultures (Fig. 1) containing similar proportions of midbrain dopaminergic neurons as previously demonstrated [25, 27]. The neurons had defined long neurites and expressed beta-TubulinIII (a marker of newly formed neurons, approximately 85%), MAP2 (a marker of mature neurons, approximately 70%), and synaptophysin (a marker of presynaptic regions). As expected, many of the neurons (approximately 35%) were also positive for tyrosine hydroxylase (TH), indicating dopaminergic identity, and FOXA2, indicating a midbrain phenotype. Moreover, the cultures



**Fig. 2 Impaired mitophagy in *PARK2* KO neurons.** **A** Investigation of mitophagy in *PARK2* KO and control neurons after CCCP treatment (10  $\mu$ M, 48 h) by immunofluorescence staining for the mitochondrial markers TOM20 (red) and HSP60 (green); Hoechst (blue) indicates nuclei. Scale bar: 20  $\mu$ m. **B** Quantification of TOM20 and HSP60 immunoreactivity. **C** Western blotting analysis for TOM20 and HSP60. Full-length blots are presented in Supplementary Materials. **D** Quantification of western blots. Expression levels were normalized to  $\alpha$ -actin and are shown relative to control/DMSO neurons (untreated). **E** Representative transmission electron microscopy (TEM) micrographs of treated (10  $\mu$ M CCCP, 48 h) and untreated neurons. Scale bar: 500 nm. **F** Quantification of mitochondria on TEM images in **E**. **G** Reactive oxygen species (ROS) levels in control and *PARK2* KO neurons after exposure (10  $\mu$ M CCCP, 48 h). **H** pS65-Ub was elevated in *PARK2* KO and control neurons after CCCP treatment (10  $\mu$ M CCCP, 48 h). pS65-Ub levels were below detection without CCCP. Data presented as mean  $\pm$  SEM,  $n = 3$ –9 technical replicates, data from 2 (**F**, **H**) or 3 (**B**, **D**, **G**) independent differentiations. Significant differences are indicated by \* $p < 0.05$ , \*\* $p < 0.01$ , \*\*\* $p < 0.001$ , ns: not significant, two-way ANOVA followed by Tukey's post hoc for multiple comparisons.

contained a population of GABA<sup>+</sup> neurons and GFAP<sup>+</sup> astrocytes (approximately 5–8%). Interestingly, the number of GFAP<sup>+</sup> cells was slightly higher in *PARK2* KO neurons compared to controls. For quantitative data on the cellular composition of the cultures, see our previous publications [25, 27].

#### Parkin deficiency results in impaired mitophagy

We have previously demonstrated increased mitochondrial area and accumulation of mitochondria with abnormal morphology in

*PARK2* KO neurons using transmission electron microscopy (TEM) [28]. The current study confirmed the increased mitochondrial area (Fig. 2A, B) in *PARK2* KO neurons compared to that of control neurons at basal growth conditions (no carbonyl cyanide *m*-chlorophenylhydrazone (CCCP)-mediated mitochondrial stress) using image quantification of immunofluorescent staining for the mitochondrial markers TOM20 and HSP60. Surprisingly, this observation was not corroborated by Western blotting (no CCCP, Fig. 2C, D); however, ultrastructural analysis showed a non-

significant tendency for an increased mitochondrial number in *PARK2* KO neurons (no CCCP, Fig. 2E, F). Moreover, the increased mitochondrial area (shown by increased TOM20+ and HSP60+ staining areas, Fig. 2A, B) in *PARK2* KO neurons correlated with elevated ROS levels (no CCCP, Fig. 2G), as reported previously by our research group [27].

To analyze whether the observed mitochondrial accumulation was associated with impaired mitophagy, we monitored the ability of the neurons to clear impaired mitochondria in response to CCCP. To optimize the mitophagy response window, neurons were treated with 10  $\mu$ M CCCP in a time-dependent manner (24, 48, 72, and 96 h) followed by quantification of nuclei and the area covered by the mitochondrial marker TOM20 (Fig. S1A–C). TOM20 area was unaffected by CCCP treatment in *PARK2* KO neurons. In control neurons, the 48 h time point gave the largest reduction in TOM20 area without affecting cell survival and was used in subsequent experiments.

Studies indicate that the loss of TOM20 staining can reflect proteolysis at the outer mitochondrial membrane by the ubiquitin-proteasome system (UPS) rather than *de facto* degradation of the mitochondria via mitophagy [29, 30]. Therefore, we quantified the area covered by both TOM20 and the mitochondrial matrix protein HSP60 in response to CCCP treatment (Fig. 2A, B) and showed that both markers decline in response to CCCP treatment in control neurons. Noticeably, the remaining mitochondrial population was positive for both TOM20 and HSP60 and, although we could observe discrete patches negative for TOM20, the TOM20 and HSP60 areas were not significantly different (Fig. 2A, B and S2). Western blotting followed by densitometric analysis confirmed the reduction in TOM20 and HSP60 proteins (Fig. 2C, D), and TEM revealed fewer mitochondria (Fig. 2E, F) in control neurons in response to CCCP, confirming clearance of CCCP-damaged mitochondria. Mitochondrial load was not decreased by CCCP treatment in *PARK2* KO neurons as indicated by TOM20 and HSP60 immunostaining (Fig. 2A, B), Western blotting (Fig. 2C, D), and TEM (Fig. 2E, F). This implies that parkin deficiency is associated with impaired mitophagy. ROS data showed CCCP-induced mitochondrial stress in both lines, confirming the induction of mitochondrial stress at the 48 h time point (Fig. 2G).

Following mitochondrial depolarization, PINK1 becomes stabilized on the outer mitochondrial membrane leading to phosphorylation of ubiquitin at serine 65 (pS65-Ub) [31]. Using Time-Resolved Fluorescence Resonance Energy Transfer (TR-FRET), we measured the pS65-Ub level in control and *PARK2* KO neurons with and without CCCP (10  $\mu$ M, 48 h). Untreated *PARK2* KO and control neurons had undetectable levels of pS65-Ub, which were strongly amplified in both cell lines after CCCP treatment (Fig. 2H). The pS65-Ub levels were significantly higher in CCCP-treated parkin-deficient neurons compared to healthy controls (Fig. 2H), potentially caused by the accumulation of damaged mitochondria in *PARK2* KO neurons.

Overall, our data show that control neurons respond to mitochondrial damage with mitophagy whereas *PARK2* KO neurons are defective in clearing impaired mitochondria.

#### USP30 inhibition facilitates mitophagy in control and *PARK2* KO neurons after mitochondrial damage with CCCP and induces basal mitophagy in *PARK2* KO neurons

USP30 counteracts parkin-mediated ubiquitination of mitochondrial outer membrane proteins, thereby inhibiting mitophagy [13, 32] (Fig. S3A). Therefore, we investigated whether USP30 inhibition could accelerate mitophagy in control and *PARK2* KO neurons after mitochondrial damage with CCCP. For this purpose, we used two structurally related small molecule USP30 inhibitors (which we term USP30i-37 and USP30i-3) synthesized based on the 1-cyano-pyrrolidine structure (Fig. S3B). According to the publicly available patent (WO2016/156816), USP30i-37 and

USP30i-3 have an  $IC_{50} < 0.1 \mu$ M for inhibition of the USP30 enzyme. We tested the potency and specificity of the compounds using the DUB profiler screening platform (Ubiquigent).  $IC_{50}$  values for USP30 inhibition were in line with data from the patent (Suppl. Materials, Table S1). The inhibitors showed good selectivity towards USP30 versus other DUBs, except for USP6, for which the inhibitors also showed some selectivity, but still not as strong as for USP30 (Suppl. Materials, Tables S1 and S2).

Western blotting confirmed that our isogenic cell lines expressed comparable levels of USP30 protein (Fig. S3C). Release of lactate dehydrogenase (LDH) and counts of cell nuclei (DAPI+ nuclei, including the morphological assessment) identified 3  $\mu$ M of the USP30 inhibitors USP30i-37 and USP30i-3 in a dose-response experiment to be non-toxic to the neurons, also in the presence of CCCP (Figs. S4–S6). Interestingly, *PARK2* KO neurons have more necrotic cells than control neurons, which is described in our previous study [25]. Moreover, 3  $\mu$ M of the USP30 inhibitors did not affect the neuronal content in the cultures i.e., no changes were observed in the numbers of MAP2+ and TH+ neurons (Fig. S5).

To assess the potential of the compounds to promote mitophagy, neurons were treated with USP30 inhibitors (0–6  $\mu$ M) for 4 h prior to CCCP exposure (10  $\mu$ M), and mitophagy was evaluated after 48 h by double immunofluorescence staining for TOM20 and HSP60 (Figs. 3A and 4A). In line with data presented in Fig. 2B, CCCP significantly decreased TOM20 and HSP60 areas in healthy control neurons (Figs. 3A, B and 4A, B) but did not reduce TOM20 and HSP60 areas in *PARK2* KO neurons (Figs. 3A, C and 4A, C).

A significant potentiation of the CCCP-induced decrease in TOM20 and HSP60 areas in control neurons was observed after treatment with 3  $\mu$ M and 6  $\mu$ M of USP30i-37 (Fig. 3B) and 6  $\mu$ M of USP30i-3 (Fig. 4B), in line with USP30 inhibition boosting mitophagy. Importantly, 3 and 6  $\mu$ M of both inhibitors boosted the CCCP-induced TOM20 and HSP60 area reduction in the *PARK2* KO neurons as well (Figs. 3A, C and 4A, C). This shows that USP30 inhibition can accelerate mitophagy in *PARK2* KO neurons even if mitochondrial damage by CCCP did not do so. In *PARK2* KO neurons, but not control neurons, 6  $\mu$ M USP30i-37 (Fig. 3C) and 6  $\mu$ M USP30i-3 (Fig. 4C) reduced TOM20 and HSP60 areas even in the absence of CCCP-induced mitochondrial damage, indicating that accumulated damaged mitochondria in the *PARK2* KO cells can be degraded in response to USP30 inhibition.

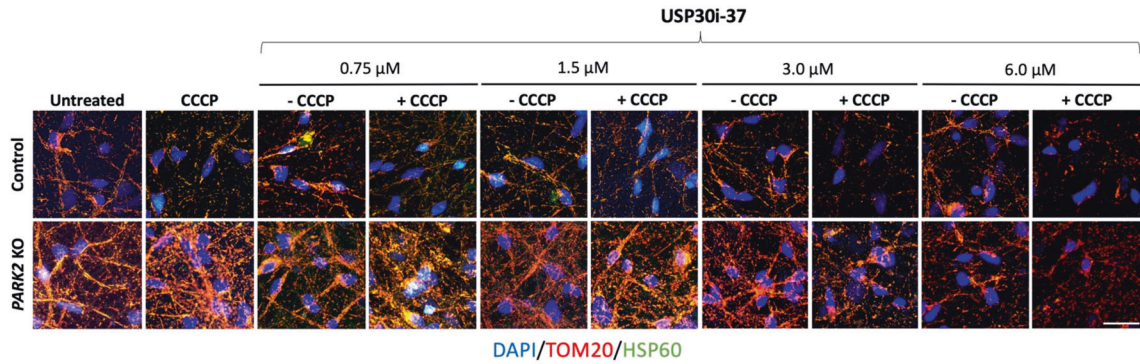
TEM analysis verified the TOM20 and HSP60 immunofluorescence data. In control neurons, but not *PARK2* KO neurons, mitochondrial abundance was reduced after CCCP treatment (Fig. 5A, B). USP30i-37 and USP30i-3 (3  $\mu$ M) enhanced mitophagy in control and *PARK2* KO neurons subjected to mitochondrial damage by CCCP (Fig. 5A, B). Data also confirmed that USP30i-37 decreased the number of mitochondria in *PARK2* KO neurons but not in control neurons, even in the absence of CCCP-induced mitochondrial damage (Fig. 5A, B).

Overall, USP30 inhibition exhibits the potential to boost mitophagy in CCCP-damaged control and *PARK2* KO neurons and to induce mitophagy at basal conditions in *PARK2* KO neurons.

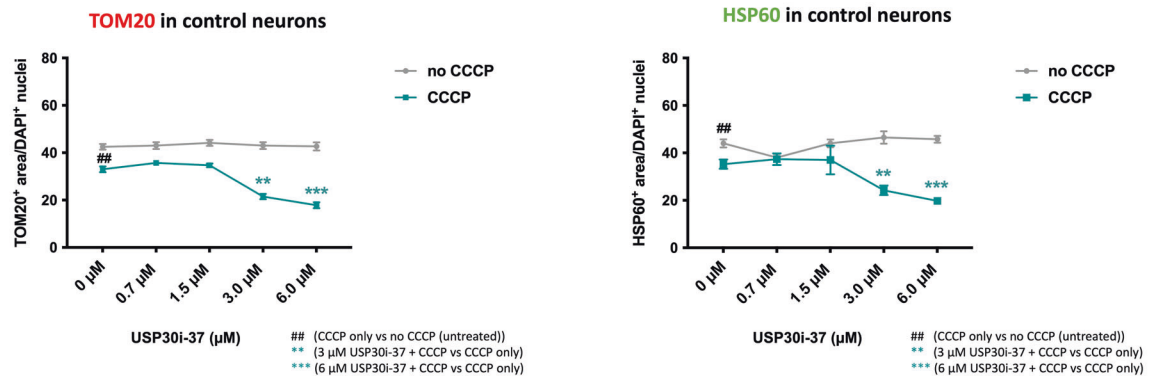
#### USP30 inhibition reduces excessive ROS production

ROS generation can cause oxidative damage to mitochondria, and the damaged mitochondria can promote further ROS generation, creating a vicious cycle that can cause cellular injury [33, 34]. Having shown that USP30 inhibition induces mitophagy, we investigated whether USP30 inhibition could reduce ROS levels. Differentiated neurons were treated with 0–6  $\mu$ M USP30i-37 or USP30i-3 with or without CCCP, and hydrogen peroxide was measured at the cell population level as an indicator of oxidative stress. In control and *PARK2* KO neurons, ROS levels significantly increased after CCCP exposure, indicating that CCCP treatment induces mitochondria-mediated oxidative stress (Fig. 6A–D).

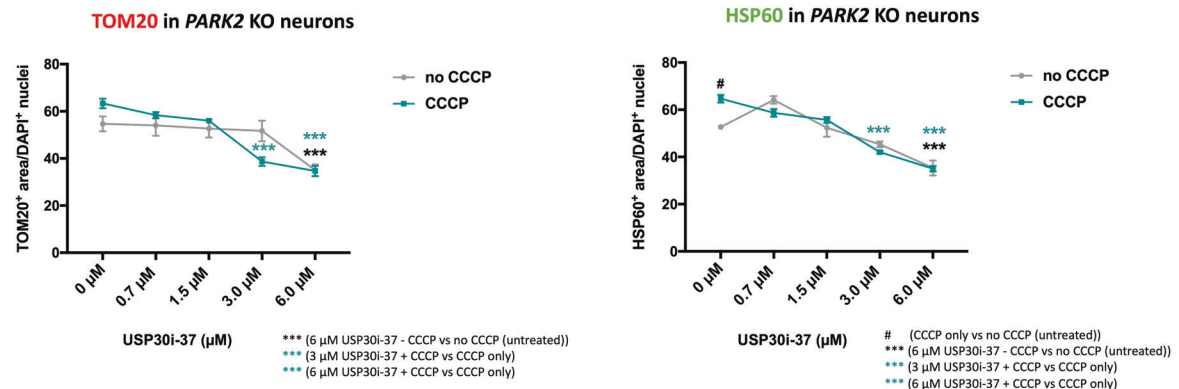
A



B



C



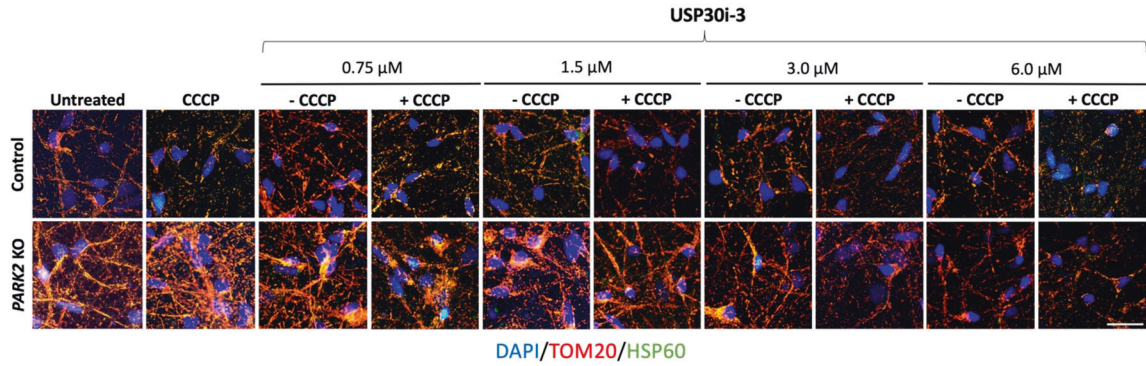
**Fig. 3 USP30 inhibition (compound 37) enhances CCCP-induced mitophagy but not basal mitophagy in control neurons and induces basal mitophagy and mitophagy of CCCP-damaged mitochondria in *PARK2* KO neurons.** **A** Immunofluorescence staining for the mitochondrial markers TOM20 (red) and HSP60 (green) after treatment with USP30 inhibitors (0.75 μM, 1.5 μM, 3 μM, 6 μM) added 4 h prior to CCCP (10 μM, 48 h). DAPI (blue) indicates nuclei. Scale bar: 50 μm. Quantification of TOM20 and HSP60 immunoreactivity upon treatment with USP30i-37 alone and in combination with CCCP in **B** control and **C** *PARK2* KO neurons. Data presented as mean ± SEM,  $n = 9$  technical replicates, data from 3 independent differentiations. Significant differences are indicated by  $^{\#}p < 0.05$ ,  $^{**}p < 0.01$ ,  $^{***}p < 0.001$ , one-way ANOVA followed by Dunnett's post hoc for multiple comparisons.

USP30i-37 (1.5, 3, and 6 μM) and USP30i-3 (3 and 6 μM in control; 1.5, 3, and 6 μM in *PARK2* KO) reduced CCCP-induced ROS levels in both cell lines (Fig. 6A–D). Interestingly, also basal ROS levels (no CCCP damage) in *PARK2* KO but not control neurons were reduced by 3 and 6 μM USP30i-37 and 6 μM USP30i-3 (Fig. 6B, D), which may be linked to the higher basal ROS levels in the mutant line (Fig. 2G). This supports that mitophagy induction by USP30 inhibition can reduce ROS levels in compromised (either by CCCP or parkin KO) neurons.

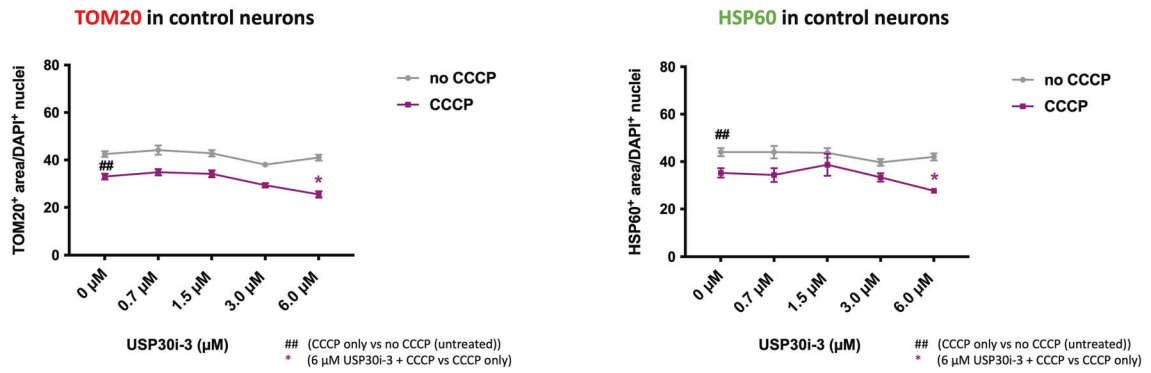
#### CCCP-induced mitophagy is impaired in both *PARK2* KO TH+ and TH- neurons, while USP30 inhibitor-induced mitophagy occurs mainly in TH- cells

Next, we investigated whether USP30 inhibitor-induced mitophagy was selective towards TH+ or TH- neuronal subtypes. *PARK2* KO neurons were exposed to 3 μM of USP30i-37 or USP30i-3, with or without CCCP (10 μM), and subsequently immunostained for HSP60 and TH. As demonstrated at the total population level (Figs. 3A, C and 4A, C), CCCP did not reduce the HSP60 area

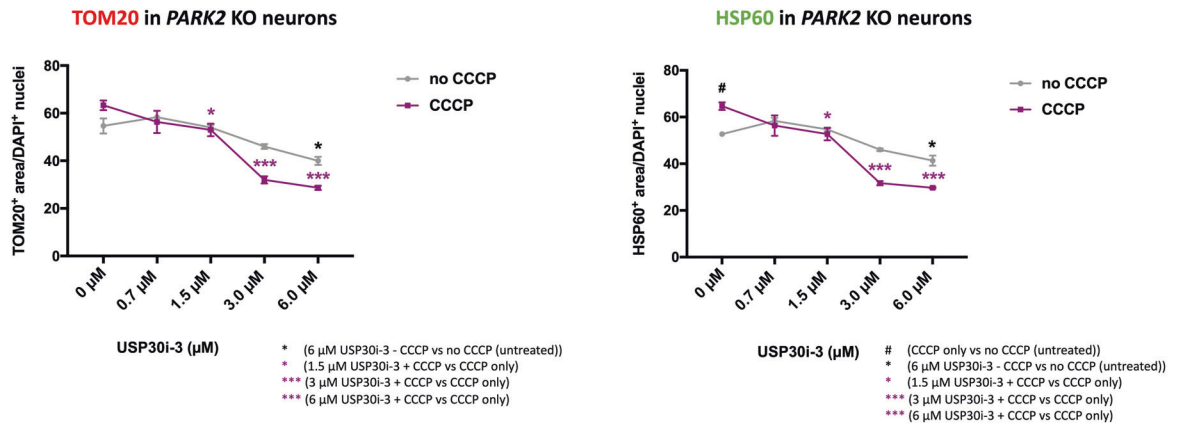
A



B



C

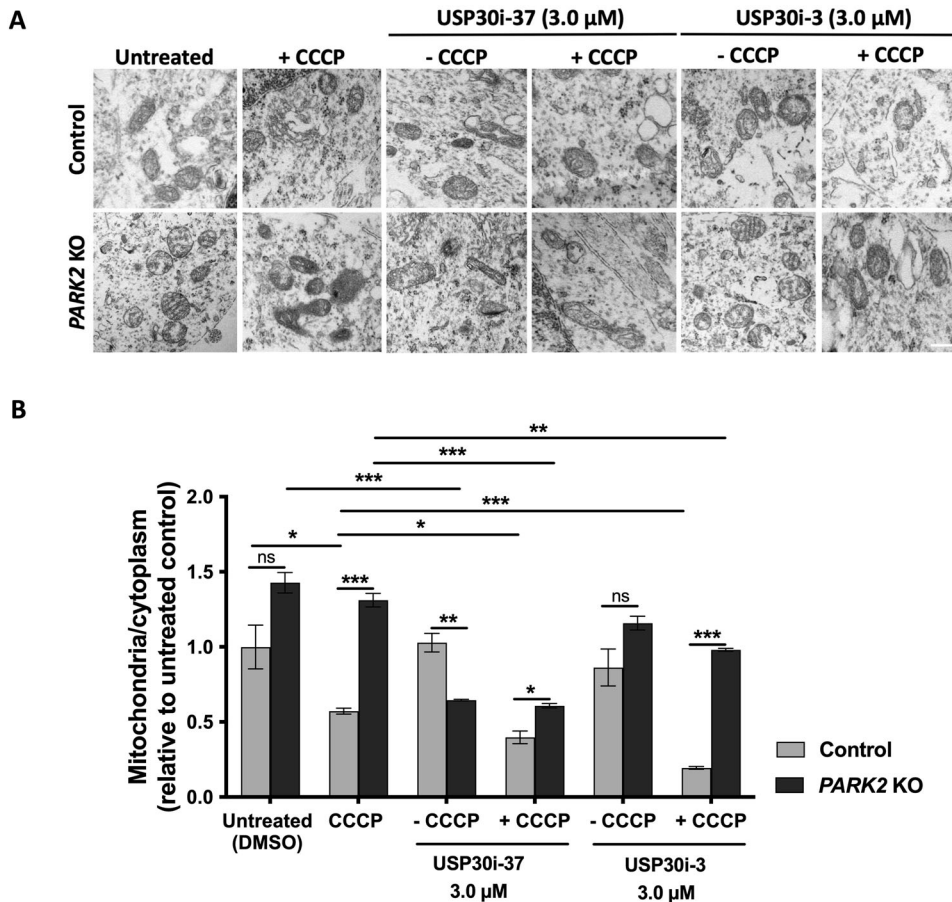


**Fig. 4 USP30 inhibition (compound 3) enhances CCCP-induced mitophagy but not basal mitophagy in control neurons and induces basal mitophagy and mitophagy of CCCP-damaged mitochondria in *PARK2* KO neurons.** **A** Immunofluorescence staining for the mitochondrial markers TOM20 (red) and HSP60 (green) after treatment with USP30 inhibitors (0.75 μM, 1.5 μM, 3 μM, 6 μM) added 4 h prior to CCCP (10 μM, 48 h). DAPI (blue) indicates nuclei. Scale bar: 50 μm. Quantification of TOM20 and HSP60 immunoreactivity upon treatment with USP30i-3 alone and in combination with CCCP in **B** control and **C** *PARK2* KO neurons. Data presented as mean ± SEM,  $n = 9$  technical replicates, data from 3 independent differentiations. Significant differences are indicated by \*, #  $p < 0.05$ , ##  $p < 0.01$ , \*\*\*  $p < 0.001$ , one-way ANOVA followed by Dunnett's post hoc for multiple comparisons.

in *PARK2* KO TH+ or TH- neurons (Fig. 7A–C), showing that mitophagy induction was impaired in both neuronal subtypes. The HSP60 area was reduced by 3 μM USP30i-3 but not USP30i-37 in both TH+ and TH- neurons after mitochondrial damage with CCCP (Fig. 7A–C). This is in line with USP30i-3 having a stronger effect than USP30i-37 at the total neuronal population level (Figs. 3 and 4). In TH-, but not TH+ neurons, 3 μM USP30i-37 and USP30i-3 reduced HSP60 areas in the absence of CCCP-induced

mitochondrial damage, demonstrating a stronger effect of USP30 inhibition on basal mitophagy in the *PARK2* KO TH- neurons. It appears that TH- cells drive the USP30 inhibitor-mediated mitophagy in the total cell population, which is in accordance with the majority of cells in the culture being TH-.

The effect of USP30 inhibition on oxidative stress was also investigated at the TH+ and TH- subpopulation levels using the fluorogenic probe CELLROX, which exhibits bright green



**Fig. 5 Transmission electron microscopy (TEM) confirms that USP30 inhibition induced mitophagy.** **A** TEM picture showing mitochondria in control and *PARK2* KO neurons after treatment with USP30i-37 and USP30i-3 (+/- CCCP). USP30 inhibitors (3  $\mu$ M) were added 4 h prior to CCCP (10  $\mu$ M, 48 h). Scale bar: 500 nm. **B** Quantification of mitochondria/cytoplasm ratios showing the relative abundance of total and abnormal mitochondria in control and *PARK2* KO neurons. Data presented as mean  $\pm$  SEM,  $n = 6$  technical replicates, data from two independent differentiations. Significant differences are indicated by \* $p < 0.05$ , \*\* $p < 0.01$ , \*\*\* $p < 0.001$ , ns: not significant, two-way ANOVA followed by Tukey's post hoc for multiple comparisons.

fluorescence upon oxidation by ROS and subsequent binding to DNA. The CCCP-induced ROS production was reduced by USP30i-37 and/or USP30i-3 in *PARK2* KO TH+ and TH- neurons (Fig. 7D–F). USP30 inhibition had no effect on basal ROS levels (no CCCP damage) in TH+ neurons (Fig. 7E) but reduced basal ROS levels in TH- neurons (Fig. 7F). This indicates that TH- neurons are the major drivers of the USP30 inhibitor-mediated reduction of basal ROS (no CCCP) in *PARK2* KO neurons (Fig. 6B, D), supporting the observation that TH- neurons represent the treatment-sensitive population.

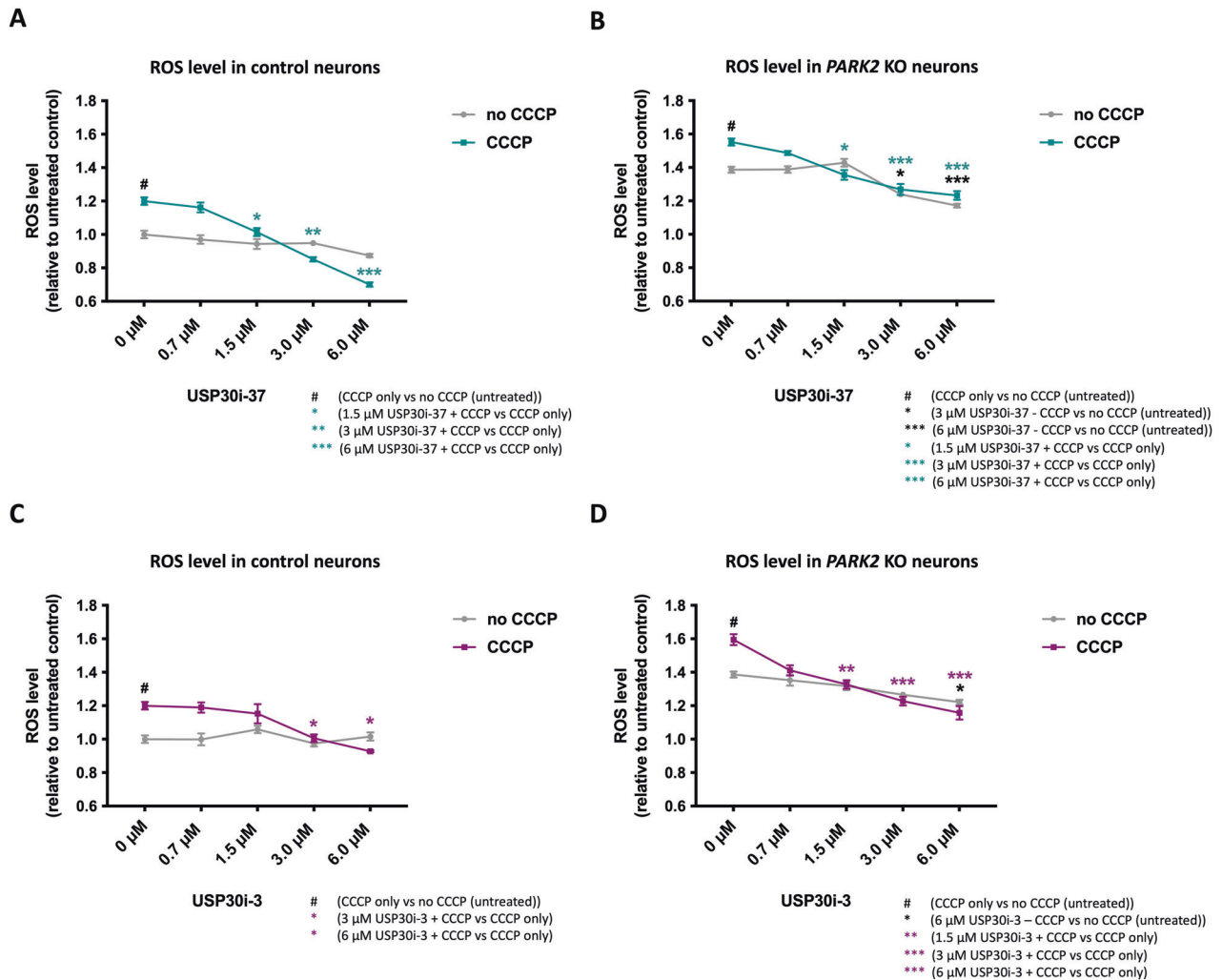
## DISCUSSION

Accumulation of damaged mitochondria in parkin mutation carriers has been proposed to be the underlying pathogenesis of various diseases as E3 ligases add ubiquitin chains to the outer mitochondrial membrane proteins to trigger mitophagic removal of aged mitochondria [35]. We used our human iPSC-derived *PARK2* KO neuronal model to investigate the impact of parkin loss on mitochondrial turnover and function under basal conditions as well as under mitochondrial stress induced by treatment with the mitochondrial uncoupler CCCP. In line with our previous data [25–28], parkin deficiency resulted in increased mitochondrial area, accumulation of mitochondria with abnormal morphology, and increased ROS levels at basal conditions as compared to control neurons [27]. In the current study, we show that *PARK2* KO

neurons are defective in clearing CCCP-impaired mitochondria. Several previous studies showed significantly impaired mitophagy in parkin-deficient cells [36–38], which correlates well with our observations of mitochondrial abnormalities and an impaired mitophagy response.

Both ubiquitin-dependent and -independent mitophagy pathways appear in the literature [20, 39]. It is unclear whether or not mitophagy in parkin mutation patients is driven by ubiquitination. Treatment with CCCP increased pS65-Ub levels in *PARK2* KO neurons, supporting the presence of ubiquitin labeling of mitochondria for degradation even in the absence of functional parkin, suggesting that another ubiquitin ligase must be in play. In fact, other E3 ubiquitin ligases, including HUWE1, MUL1, MARCH5 have been reported to regulate mitophagy [40–42].

USP30 inhibition has been suggested as a therapeutic approach to facilitate ubiquitination-driven mitophagy in neurodegenerative diseases [13, 43, 44]. Our demonstration that mitochondria are labeled with ubiquitin following the CCCP challenge in *PARK2* KO neurons (presented in Fig. 2F) is important as it highlights USP30 as a valid pharmacological target. As shown in this study, inhibition of USP30 appears to facilitate mitophagy. This is in line with the demonstration of pS65-Ub in *PARK2* KO mice and *PARK2* KO HEK cells [45, 46], but in contrast to the finding of negligible p-S65-Ub levels in human fibroblasts carrying heterozygote parkin mutations [20]. Differences may be due to the cell types, the sensitivity of the pS65-Ub



**Fig. 6 USP30 inhibition reduces excessive ROS production.** Measurement of cellular  $H_2O_2$  levels after USP30 inhibitors treatment (0.75  $\mu$ M, 1.5  $\mu$ M, 3  $\mu$ M, 6  $\mu$ M) added 4 h prior to CCCP (10  $\mu$ M, 48 h) in **A** control and **B** *PARK2* KO neurons treated with inhibitor USP30i-37, **C** control and **D** *PARK2* KO neurons treated with inhibitor USP30i-3. Data presented as mean  $\pm$  SEM,  $n = 12$  technical replicates, data from 3 independent differentiations. Significant differences are indicated by \* $p < 0.05$ , \*\* $p < 0.01$ , \*\*\* $p < 0.001$ , one-way ANOVA followed by Dunnett's post hoc test for multiple comparisons.

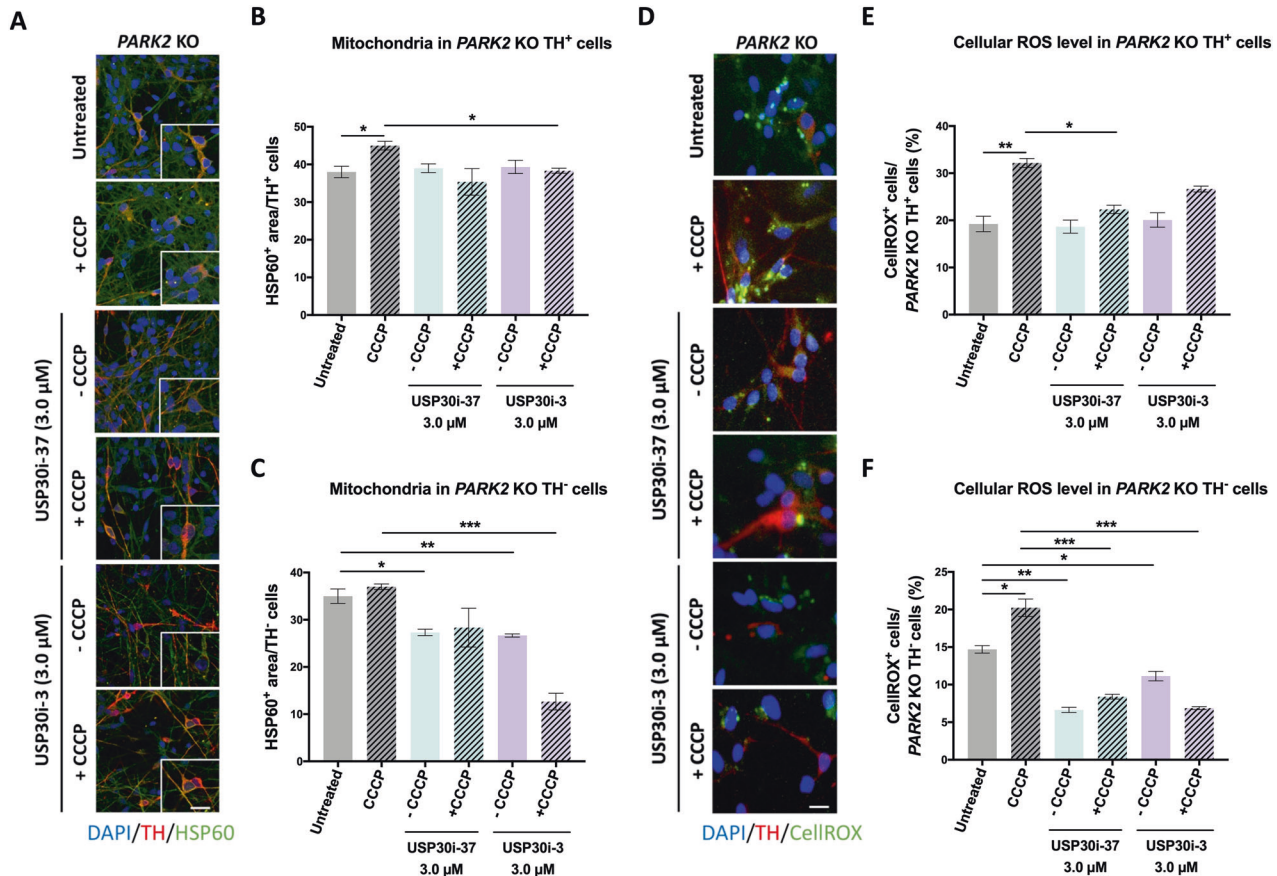
assays, or the mitochondria decoupler treatment paradigms. To gain a more comprehensive understanding of our data, extensive supplementary experiments are needed. Such experiments could involve investigations at additional time points and immunofluorescence staining using selective antibodies to identify specific neuronal subtypes exhibiting pS65-Ub accumulation in *PARK2* KO cultures.

In our study, we used two 1-cyano-pyrrolidine derivatives at doses of 0.75  $\mu$ M, 1.5  $\mu$ M, 3  $\mu$ M, 6  $\mu$ M as USP30 inhibitors. The first study involving pharmacological inhibition of USP30 was documented by Phu et al. in 2020 [17], and subsequently, Rusilowicz-Jones et al. [18] in the same year reported a first cyano-pyrrolidine compound, exhibiting a USP30 selectivity profile similar to the compounds used in our study. Their research demonstrated the enhancement of TOM20 ubiquitylation and the induction of mitophagy in human SHSY5Y cells at a concentration of 200 nM of USP30 inhibitor [18]. Furthermore, Tsefou et al. 2021 also reported the effective use of a compound derived from 1-cyano-pyrrolidine in parkin mutant fibroblasts, administering doses ranging from 0.1  $\mu$ M to 10  $\mu$ M [20]. Discrepancies in dosage between studies may result from the use of different cell models and variations in the specific cyano-pyrrolidine derivatives employed.

In our neuronal in vitro model, we found that USP30 inhibitors boosted CCCP-induced mitophagy in control neurons. This supports previous studies reporting enhanced CCCP-induced TOM20 and HSP60 reduction in USP30-depleted or USP30 KD cells [13, 19, 32]. Interestingly, our data indicate that USP30 inhibition facilitates mitophagy in parkin-deficient neurons at both basal growth conditions and upon CCCP stress. In line with this, USP30 inhibition increases mitophagy in induced neurons derived from parkin loss-of-function carriers [47]. Moreover, defective mitophagy in SH-SY5Y cells transfected with PD-linked parkin mutants can be rescued with siRNA-mediated KD of USP30 and USP15 [13, 48]. In contrast, TOM20 reduction by USP30 inhibition requires parkin in HeLa cells [21].

We used our model system with *PARK2* KO or CCCP-induced mitochondrial impairment to investigate whether mitophagy induction by USP30 inhibition would lead to a healthier cellular environment. We found that parkin-deficient and/or CCCP-treated neurons generated more ROS than control cells and that USP30 inhibition reduced the level of oxidative stress. Overall, this indicates that USP30 inhibition can reduce ROS production, presumably by inducing mitophagy whereby damaged ROS-producing mitochondria are removed [49–51]. Consistent with our





**Fig. 7 TH-negative neurons are the major driver of USP30 inhibitor-mediated mitophagy and ROS reduction in *PARK2* KO cells.** **A** Immunofluorescence staining for the mitochondrial marker HSP60 (green) and the catecholaminergic marker TH (red) after treatment with USP30i-37 and USP30i-3 (3 μM) added 4 h prior to CCCP (10 μM, 48 h). DAPI (blue) indicates nuclei. Scale bar: 50 μm. Quantification of HSP60 area upon USP30i-37 and USP30i-3 in **B** *PARK2* KO TH+ neurons ( $n = 115$ – $125$ ) and **C** *PARK2* KO TH- cells ( $n = 333$ – $343$ ). **D** Cellular ROS levels measured by CellROX Reagent (green) on catecholaminergic neurons (TH (red)) after treatment with USP30i-37 and USP30i-3 (3 μM) added 4 h prior to CCCP (10 μM, 48 h). DAPI (blue) indicates nuclei. Scale bar: 50 μm. Quantification of CellROX levels upon USP30i-37 and USP30i-3 treatment in **E** *PARK2* KO TH+ neurons ( $n = 98$ – $105$ ) and **F** *PARK2* KO TH- neurons ( $n = 258$ – $265$ ). Data presented as mean  $\pm$  SEM,  $n = 9$  technical replicates from 3 independent differentiations. Significant differences are indicated by \* $p < 0.05$ , \*\* $p < 0.01$ , \*\*\* $p < 0.001$ , one-way ANOVA followed by Dunnett's post hoc test for multiple comparisons.

study, there are other papers that have also previously reported the beneficial effects of USP30 inhibition on mitochondrial parameters. Bingol et al. 2014 have shown that USP30 KD leads to a healthier cellular environment (reduced oxidative stress in primary neurons and restoration of mitochondrial defects in drosophila PINK1 and parkin mutant flies) [13]. Rusilowicz-Jones et al. 2021 have described a selective USP30 inhibitor that showed a potency to restore basal mitophagy and membrane potential in dopaminergic neurons generated from PD patient fibroblasts [47]. An important novelty of the current paper is the confirmation of these findings in another human model system, using novel compounds, and the demonstration of the non-dopaminergic neurons being the main drivers of the beneficial effects of USP30 inhibition. In addition, our data support the limited evidence for a beneficial cellular effect of mitophagy induction by USP30 inhibition, pointing to USP30 inhibition as a potential therapeutic approach.

We show that USP30 inhibition induces mitophagy and reduces excessive ROS levels even in neurons that lack functional parkin, suggesting that USP30 also opposes parkin-independent mitophagy. The enhancement of mitophagy through USP30 inhibition shown in this study is consistent with findings from previous research [20, 44, 47], while the observed normalization of elevated ROS levels is a novel aspect of our study. CCCP-induced pS65-Ub

levels were significantly higher in *PARK2* KO compared to control neurons, but *PARK2* KO neurons failed to induce mitophagy upon CCCP stress, pointing to the absence of mitophagy induction solely by the total ubiquitinate load as previously proposed [36]. One possible explanation could be that in the absence of the protein parkin, the peak amplitude of the pS65-Ub signal that initiates mitophagy is further reduced, such that only a small fraction of mitochondria can be tagged for degradation [9, 37]. However, one could also speculate that the polyubiquitin chains linkage-type, which could be different when other E3 ligases substitute for parkin, has a modulating effect on the potentiation of mitophagy [52].

Immunostaining for TH allowed us to investigate effects in TH+ and TH- neuronal subtypes in the dopaminergic differentiated cultures. While control neurons of both subtypes responded to CCCP damage with mitochondrial degradation, mitophagy was impaired in *PARK2* KO neurons of both subtypes. *PARK2* KO TH- neurons were more responsive to USP30 inhibition than TH+ neurons as they were the major drivers of mitophagy and ROS reduction. Although our data set does not indicate a strong beneficial effect of USP30 inhibition for TH+ neurons, it remains to be seen whether USP30 inhibition is capable of improving dopaminergic cell survival in vivo, where cell-to-cell interaction is more diverse and complex than in the in vitro model.

Our findings align with and support the existing body of literature, suggesting that a) USP30 inhibition can enhance mitophagy, and b) that this effect is present even in parkin-deficient cells. Notably, these findings have been reported previously, employing KD or KO approaches, orthologous assays as well as pharmacological inhibition [13, 17–20, 32, 44, 47], thus reinforcing the robustness of our results. The novelty of our study lies in the use of isogenic human iPSCs with *PARK2* KO, enabling us to investigate the specific effects of USP30 inhibitors within a unique genetic context. Furthermore, the protocol employed in our study generates a heterogeneous neuronal culture, enabling side-by-side comparisons of TH+ and TH- neurons, which is a distinctive feature of our research. In addition, our study contributes to the field by measuring the impact of USP30 inhibition on ROS levels within this unique experimental setting. This novel aspect of our research provides important insights into the broader implications of mitophagy modulation.

While our research demonstrates several notable strengths, it is also essential to be aware of the study's limitations. Our study is based on the use of a single isogenic cell line (control vs. *PARK2* KO). While employing this approach, there is the possibility of potential cellular drift over time. Nonetheless, it is important to emphasize that the applied experimental setup is well-established and validated. Another limitation of this study is that the assessment of mitophagy relies solely on monitoring mitochondrial mass. In order to further enhance the depth of our understanding, future research could consider conducting a more comprehensive analysis of mitophagy involving additional markers or assays, and a parkin rescue experiment could be included.

In conclusion, our results support USP30 inhibition as a promising approach for promoting the mitophagy of unhealthy mitochondria and reducing excessive cellular ROS production. Moreover, the approach seems valid in parkin-deficient cells. Although the *in vivo* effect on dopaminergic neurons in PD remains to be shown, the strategy could not only find applications in PD but also in other diseases with cellular dysfunction mediated by mitochondrial impairment.

## MATERIALS AND METHODS

### *In vitro* propagation and differentiation of neural stem cells (NSCs)

We analyzed two isogenic neural stem cell (NSC) lines derived from induced pluripotent stem cells (iPSCs). A healthy control iPSC line was produced by reprogramming of CD34+ cord blood cells using episomal vectors (XCell Science Inc. (Novato, CA, USA)). A *PARK2* compound heterozygous KO iPSC line was then generated from the control line using zinc finger technology. The two isogenic iPSC lines were characterized and predifferentiated to NSCs as described elsewhere (Shaltouki et al. [24]).

NSCs were propagated according to well-established, standard protocols using Geltrex-(ThermoFisher)-coated plates in Neurobasal Medium (ThermoFisher) supplemented with NEAA, GlutaMax-I, B27, supplement (ThermoFisher), penicillin-streptomycin, and bFGF. Cells were enzymatically passaged with Accutase (ThermoFisher) when 80–90% confluent. NSCs were differentiated according to a commercially available dopaminergic differentiation kit (XCell Science Inc.) for at least 25 days. Differentiation was divided into two parts: an induction phase, where NSCs were differentiated into dopaminergic precursors, and a maturation phase, where the dopaminergic precursor cells were differentiated into mature dopaminergic neurons. The differentiations were carried out at 37 °C in a low, physiological O<sub>2</sub> environment (5% CO<sub>2</sub>, 92% N<sub>2</sub>, and 3% O<sub>2</sub>). The cells were seeded onto wells coated with poly-L-ornithine (Sigma) and laminin (ThermoFisher) at a density of 50,000 cells/cm<sup>2</sup>. Complete DOPA Induction Medium (XCell Science Inc.) supplemented with 200 ng/ml human recombinant Sonic Hedgehog (Peprotech) was changed every second day for the first nine days of differentiation. The cells were passaged on day 5 and day 10 and seeded at a desired cell density. The medium was switched to Complete DOPA Maturation Medium A and B (XCell Science Inc.) on days 10 and 16, respectively. The generated neuronal populations were used for subsequent analyses.

### Treatments used

20 mM stock solution of cyanide *m-chlorophenylhydrazone* (CCCP, Sigma-Aldrich) was prepared by dissolving in dimethyl sulfoxide (DMSO) (Sigma-Aldrich) and further dilution to a final concentration of 10 μM. Cells were treated with CCCP in a time-dependent manner (24, 48, 72, and 96 h) to determine the optimal time; 48 h of exposure for further experiments was chosen.

USP30 inhibitors were derived from patent WO2016/156816 and synthesized in-house. USP30i-3 is the R-enantiomers of Example 3 and USP30i-37 is Example 37 in WO2016/156816. 100 mM stock solutions were prepared by dissolving in DMSO and further dilution in media to achieve final concentrations. USP30 inhibitor (0.75 μM, 1.5 μM, 3 μM, 6 μM) was added 4 h before addition of CCCP (10 μM).

All solutions were prepared on the day of the experiment. DMSO was used as a vehicle in all experiments and was included as an untreated control (0 μM) (at 0.1% final concentration (v/v)).

### USP30 inhibitors concentration-response

To determine the highest non-toxic dose of the tested USP30 inhibitors, cells were differentiated as previously described for 36 days. At day 34 the cells were treated with 0 μM, 1.5 μM, 3 μM, 6 μM of USP30i-37 and USP30i-3 dissolved in DMSO. Cells treated with DMSO alone served as control. At day 36, cells were analyzed using lactate dehydrogenase (LDH) assay and stained for nuclei (DAPI) and neuronal markers (MAP2 and beta-TubulinIII).

### Assessment of cytotoxicity (LDH assay)

To assess the cytotoxicity of the USP30 inhibitors in the tested doses, we used LDH assay to evaluate the content of necrotic cells. LDH assay was performed using CytoTox 96 Non-Radioactive Cytotoxicity Assay Kit (Promega) according to the manufacturer's protocol. Briefly, cells were plated in 96-well plates (40,000 cells/well), and the absorbance was recorded at 490 nm using a microplate reader (VMAX kinetic ELISA).

### Western blotting

Western blotting was performed using standard techniques. In brief, the cells were lysed on ice in phosphate-buffered saline (PBS) containing phosphatase (PhosphoSTOP Tablet, Roche) and protease (Complete Mini Tablets, Roche) inhibitors supplemented with 1% Triton-X-100 (Sigma). Samples were then sonicated for 3×10 sec at an amplitude 2 microns on ice, and the supernatants were collected. Protein content was measured with bicinchoninic acid assay (BCA, Pierce). Samples were equalized according to the protein concentration, denatured for 10 min in NuPAGE loading buffer, and separated by SDS-PAGE on NuPage 4–12% Bis-Tris gel (NuPAGE) at 200 V for 50 min with MOPS running buffer (NuPAGE). The proteins separated through iBlot transfer system (Invitrogen) were transferred onto polyvinylidene difluoride (PVDF) membranes (Invitrogen) followed by blocking the membranes for 60 min at 4 °C with 5% non-fat dry milk in a mixture of 0.05 M Tris-Buffered Saline (TBS) and 0.05% Tween-20. The membranes were incubated overnight at 4 °C in a solution containing the relevant primary antibodies. Subsequently, blots were incubated with an appropriate horseradish peroxidase (HRP)-conjugated secondary antibody for 1 h at RT. Protein expression was detected with ECL reagents (ThermoFisher) using the ChemiDoc MP imaging system (BioRad) and quantified by densitometry using Image Lab software (BioRad).

**Primary antibodies.** mouse anti-Parkin (Cell Signalling #4211) 1:1000, mouse anti-USP30 (Abcam #AB3600) 1:500, rabbit anti-TOM20 (Santa Cruz #SC-11415) 1:1000, goat anti-HSP60 (Santa Cruz Biotechnology #SC-1052) 1:200, mouse anti-α-actin (Chemicon/Millipore #MAB1501) 1:6000.

**Secondary antibodies.** HRP-conjugated anti-mouse (DAKO #P0260) 1:2000, HRP-conjugated anti-rabbit (DAKO #P0790) 1:2000, HRP-conjugated anti-goat (Millipore #AP180P) 1:2000.

### Assessment of mitophagy

Cells were treated with 10 μM CCCP for 48 h to trigger mitophagy, and the process was evaluated by immunofluorescence staining for TOM20 (outer mitochondrial membrane marker) and HSP60 (mitochondrial matrix marker).

### Immunofluorescence staining

Cells cultured in 24- or 48-well plates (Corning) containing coverslips were fixed for 20 min at room temperature (RT) in 4% (w/v) paraformaldehyde

(PFA, Sigma) in 0.15 M phosphate buffer (potassium dihydrogen phosphate (Merck) and disodium phosphate (Merck)), pH 7.4, and rinsed with 0.05 M TBS, pH 7.4, with 0.1% Triton-X-100 (Sigma). Cells were permeabilized, and unspecific binding was blocked with TBS containing 10% goat serum (Millipore) or donkey serum (Millipore) according to the host of the secondary antibodies. Cells were incubated overnight at 4 °C with primary antibodies diluted in TBS/10% goat or donkey serum. Cultures were rinsed in TBS/0.1% Triton-X-100 and incubated with an appropriate secondary antibody diluted 1:500 in TBS/10% goat serum for 2 h at RT. Cell nuclei were counterstained with 10  $\mu$ M 4',6-diamidino-2-phenylindole dihydrochloride (DAPI, Sigma) or Hoechst 33342 (Sigma) in TBS. Cultures were mounted onto glass slides with ProLong Diamond mounting medium (Molecular Probes).

**Primary antibodies.** mouse anti- $\beta$ -tubulin (Sigma #T8660; 1:2000), mouse anti-microtubule-associated protein 2a+b (MAP2, Sigma #M1406; 1:2000), rabbit anti-tyrosine hydroxylase (TH, Millipore #AB152; 1:600), mouse anti-synaptophysin (Sigma #S5768; 1:200), goat anti-forkhead box A2 (FOXA2 (Sigma #AF2400; 1:250), rabbit anti-GABA (Sigma #A2052; 1:2000), rabbit anti-GFAP (DAKO #Z0334; 1:4000), rabbit anti-TOM20 (Santa Cruz #SC-11415, 1:1000), goat anti-HSP60 (Santa Cruz Biotechnology #SC-1052, 1:200).

**Secondary antibodies.** Alexa Fluor 555 goat anti-mouse IgG (Molecular Probes #A21422, 1:500), Alexa Fluor 594 donkey anti-goat (ThermoFisher #A11058, 1:500), Alexa Fluor 488 goat anti-rabbit IgG (ThermoFisher #A11008, 1:500), Alexa Fluor 488 donkey anti-goat IgG (Invitrogen #A11055, 1:500).

### Image analysis

Fluorescence pictures were taken using a FluoView FV1000MPE—Multiphoton Laser Confocal Microscope (Olympus) 60x magnification, in a blinded manner on 5 randomly chosen confocal fields per coverslip from independent experiments. Mitophagy was analyzed by quantifying the total area of TOM20+ and HSP60+ stainings. The analysis was performed automatically in ImageJ Software by converting images to binary format and analyzing particles. The total area of TOM20+ and HSP60+ stainings was normalized to the total cell numbers as quantified automatically in ImageJ for Hoechst+/DAPI+ nuclei.

### Transmission electron microscopy (TEM)

Cells were seeded on 13 mm Thermanox plastic coverslips (Nunc) coated with poly-L-ornithin/laminin, primarily fixed in 3% glutaraldehyde (Merck) in 0.1 M sodium phosphate buffer with pH 7.2 at 4 °C for 1 h, and stored in a 0.1 M Na-phosphate buffer at 4 °C until further analysis. When ready, the cells were embedded in 4% agar at 45 °C (Sigma) under the stereomicroscope and cut into 1–2 mm<sup>3</sup> blocks, which were then washed with 0.1 M Na-phosphate buffer followed by post-fixation in 1% osmium tetroxide in 0.1 M Na-phosphate buffer (pH 7.2) for 1 h at RT. Cells were washed in MilliQ water, followed by stepwise dehydration in a series of ascending ethanol concentrations ranging from 50–99% EtOH. Propylene oxide (Merck) was then used as an intermediate to allow infiltration with Epon (812 Resin, TAAB). The following day, the agar blocks were placed in flat molds in pure Epon, and cured at 60 °C for 24 h. Approximately eight semi-thin sections (2  $\mu$ m) from one block were cut on an ultramicrotome with a glass knife (Leica, Reichert Ultracut UTC). These were stained with 1% toluidine blue in 1% Borax and evaluated by light microscopy to locate areas with an adequate number of cells for further processing. Ultra-thin sections (70 nm) were cut on the ultramicrotome with a diamond knife (Jumdi, 2 mm) and then collected onto TEM copper grids (Gilder) and stained with 2% uranyl acetate (Polyscience) and 1% lead citrate (Reynolds 1963). The samples were evaluated, and the images were collected using a Philips CM100 transmission electron microscope equipped with Morada digital camera equipment and iTEM software system.

### Morphometric analysis of TEM images

Six TEM grids from each cell line were used for analysis, and ten spots were randomly chosen at low magnification. Images of each spot were captured using high magnification (19,000X). To estimate mitochondrial abundance, the organelles were counted manually on each micrograph and normalized to the cytoplasm area. Thirty images were used for each cell line.

### Phospho-Ubiquitin (Ser65) assay

Phosphorylated Ubiquitin at Ser65 levels was measured using the Time-Resolved Fluorescence Resonance Energy Transfer (TR-FRET) Phospho-

Ubiquitin (Ser65) Cellular Kit (Cisbio 64UBIS65PEG) according to the manufacturer's instructions. Briefly, cells were plated in a 96-well plate (60,000 cells/well) and lysed using lysis buffer for the kit. Cell lysate samples were transferred into a new plate, and Activation Buffer was added together with Mix Detection Antibodies (the kit included positive and negative controls). The plate was incubated for 1 h at RT and read on an HTRF plate reader (Molecular Devices).

### Measurement of oxidative stress levels

**ROS assay.** ROS level was measured using ROS-Glo™ H<sub>2</sub>O<sub>2</sub> Assay Kit (Promega) according to the manufacturer's instructions. Briefly, cells were plated in a 96-well plate (5,000 cells/well). Media were transferred to a new 96-well plate, and the H<sub>2</sub>O<sub>2</sub> substrate was added to each media sample and incubated for 1 h at 37 °C. The ROS-Glo™ Detection Solution was then added, the plate was incubated for an additional 20 min at RT, and the luminescence signal was recorded using an Orion L Microplate Luminometer (Titertek Berthold).

**CellROX assay.** Cellular ROS levels were measured using CellROX™ Green Reagent (ThermoFisher, Invitrogen) according to the manufacturer's instructions. Briefly, cells were plated in a 96-well plate (40,000 cells/well). The CellROX Reagent was added to the cells at a final concentration of 5  $\mu$ M, and the plate was incubated for 30 min at 37 °C. The medium was removed, and the cells were washed 3 times with PBS. Cells were fixed with 4% PFA for 10 min and stained for DAPI and TH. Images were generated within 24 h using ImageXpress Pico Automated Cell Imaging System (Molecular Devices). Image analysis was performed using the ImageJ software by quantifying the number of CellROX+ cells and normalizing them to the number of TH+ or TH- cells.

### Statistical analysis

Statistical analysis was performed using GraphPad Prism 7.0 software. We applied two-tailed unpaired Student's t-test and one- or two-way ANOVA with multiple comparison tests. Data were considered statistically significant at  $p < 0.05$  (\*, #),  $p < 0.01$  (\*\*, ##), and  $p < 0.001$  (\*\*\*, ###). Data are presented as mean  $\pm$  standard error of the mean (SEM).

### Reporting summary

Further information on research design is available in the Nature Research Reporting Summary linked to this article.

### DATA AVAILABILITY

The datasets used and/or analyzed during the current study are available from the corresponding author on request.

### REFERENCES

- Poewe W, Seppi K, Tanner CM, Halliday GM, Brundin P, Volkman J, et al. Parkinson disease. *Nat Rev Dis Primers*. 2017;3:17013.
- Rizek P, Kumar N, Jog MS. An update on the diagnosis and treatment of Parkinson disease. *CMAJ*. 2016;188:1157–65.
- Armstrong MJ, Okun MS. Diagnosis and treatment of Parkinson disease: a review. *JAMA*. 2020;323:548–60.
- Delamarre A, Meissner WG. Epidemiology, environmental risk factors and genetics of Parkinson's disease. *Presse Med*. 2017;46:175–81.
- Arkinson C, Walden H. Parkin function in Parkinson's disease. *Science*. 2018;360:267–8.
- Dawson TM, Dawson VL. The role of Parkin in familial and sporadic Parkinson's disease. *Mov Disord*. 2010;25:S32–9.
- Reed X, Bandrés-Ciga S, Blauwendraat C, Cookson MR. The role of monogenic genes in idiopathic Parkinson's disease. *Neurobiol Dis*. 2019;124:230–9.
- Eiyama A, Okamoto K. PINK1/Parkin-mediated mitophagy in mammalian cells. *Curr Opin Cell Biol*. 2015;33:95–101.
- Onishi M, Yamano K, Sato M, Matsuda N, Okamoto K. Molecular mechanisms and physiological functions of mitophagy. *EMBO J*. 2021;40:e104705.
- Cornelissen T, Vilain S, Vints K, Goukko N, Verstreken P, Vandenbergh W. Deficiency of parkin and PINK1 impairs age-dependent mitophagy in *Drosophila*. *Elife*. 2018;7:e35878.
- Quinn PMJ, Moreira PI, Ambrósio AF, Alves CH. PINK1/PARKIN signalling in neurodegeneration and neuroinflammation. *Acta Neuropathol Commun*. 2020;8:189.
- Garza-Lombó C, Pappa A, Panayiotidis MI, Franco R. Redox homeostasis, oxidative stress and mitophagy. *Mitochondrion*. 2020;51:105–17.

13. Bingol B, Tea JS, Phu L, Reichelt M, Bakalarski CE, Song Q, et al. The mitochondrial deubiquitinase USP30 opposes parkin-mediated mitophagy. *Nature*. 2014;510:370–5.
14. Müller L, Kutzner CE, Balaji V, Hoppe T. In vitro analysis of E3 ubiquitin ligase function. *J Vis Exp*. 2021;171:e62393.
15. Wang Y, Serricchio M, Jauregui M, Shanbhag R, Stoltz T, Di Paolo CT, et al. Deubiquitinating enzymes regulate PARK2-mediated mitophagy. *Autophagy*. 2015;11:595–606.
16. Ordureau A, Paulo JA, Zhang J, An H, Swatek KN, Cannon JR, et al. Global landscape and dynamics of parkin and usp30-dependent ubiquitylomes in iNeurons during mitophagic signaling. *Mol Cell*. 2020;77:1124–1142.e10.
17. Phu L, Rose CM, Tea JS, Wall CE, Verschueren E, Cheung TK, et al. Dynamic regulation of mitochondrial import by the ubiquitin system. *Mol Cell*. 2020;77:1107–1123.e10.
18. Rusilowicz-Jones EV, Jardine J, Kallinos A, Pinto-Fernandez A, Guenther F, Giurandino M, et al. USP30 sets a trigger threshold for PINK1-PARKIN amplification of mitochondrial ubiquitylation. *Life Sci Alliance*. 2020;3:e202000768.
19. Liang JR, Martinez A, Lane JD, Mayor U, Clague MJ, Urbé S. USP30 deubiquitylates mitochondrial Parkin substrates and restricts apoptotic cell death. *EMBO Rep*. 2015;16:618–27.
20. Tsefou E, Walker AS, Clark EH, Hicks AR, Luft C, Takeda K, et al. Investigation of USP30 inhibition to enhance Parkin-mediated mitophagy: tools and approaches. *Biochem J*. 2021;478:4099–118.
21. Luo H, Grigman J, Zhang R, Yang M, Sun N. Pharmacological inhibition of USP30 activates tissue-specific mitophagy. *Acta Physiol (Oxf)*. 2021;232:e13666.
22. Bahmad H, Hadadeh O, Chamaa F, Cheaito K, Darwish B, Makkawi AK, et al. Modeling human neurological and neurodegenerative diseases: from induced pluripotent stem cells to neuronal differentiation and its applications in neurotrauma. *Front Mol Neurosci*. 2017;10:50.
23. McComish SF, Caldwell MA. Generation of defined neural populations from pluripotent stem cells. *Philos Trans R Soc Lond B Biol Sci*. 2018;373:20170214.
24. Shaltouki A, Sivapatham R, Pei Y, Gerencser AA, Momčilović O, Rao MS, et al. Mitochondrial alterations by PARKIN in dopaminergic neurons using PARK2 patient-specific and PARK2 knockout isogenic iPSC lines. *Stem Cell Rep*. 2015;4:847–59.
25. Bogetofte H, Jensen P, Ryding M, Schmidt SI, Okarmus J, Ritter L, et al. PARK2 mutation causes metabolic disturbances and impaired survival of human iPSC-derived neurons. *Front Cell Neurosci*. 2019;13:297.
26. Bogetofte H, Jensen P, Okarmus J, Schmidt SI, Agger M, Ryding M, et al. Perturbations in RhoA signalling cause altered migration and impaired neurogenesis in human iPSC-derived neural cells with PARK2 mutation. *Neurobiol Dis*. 2019;132:104581.
27. Okarmus J, Bogetofte H, Schmidt SI, Ryding M, García-López S, Ryan BJ, et al. Lysosomal perturbations in human dopaminergic neurons derived from induced pluripotent stem cells with PARK2 mutation. *Sci Rep*. 2020;10:10278.
28. Okarmus J, Havelund JF, Ryding M, Schmidt SI, Bogetofte H, Heon-Roberts R, et al. Identification of bioactive metabolites in human iPSC-derived dopaminergic neurons with PARK2 mutation: altered mitochondrial and energy metabolism. *Stem Cell Rep*. 2021;16:1510–26.
29. Chan NC, Salazar AM, Pham AH, Sweredoski MJ, Kolawa NJ, Graham RL, et al. Broad activation of the ubiquitin-proteasome system by Parkin is critical for mitophagy. *Hum Mol Genet*. 2011;20:1726–37.
30. Yoshii SR, Kishi C, Ishihara N, Mizushima N. Parkin mediates proteasome-dependent protein degradation and rupture of the outer mitochondrial membrane. *J Biol Chem*. 2011;286:19630–40.
31. Fiesel FC, Ando M, Hudec R, Hill AR, Castanedes-Casey M, Caulfield TR, et al. (Patho-)physiological relevance of PINK1-dependent ubiquitin phosphorylation. *EMBO Rep*. 2015;16:1114–30.
32. Bingol B, Sheng M. Mechanisms of mitophagy: PINK1, Parkin, USP30 and beyond. *Free Radic Biol Med*. 2016;100:210–22.
33. Fan P, Xie XH, Chen CH, Peng X, Zhang P, Yang C, et al. Molecular regulation mechanisms and interactions between reactive oxygen species and mitophagy. *DNA Cell Biol*. 2019;38:10–22.
34. Song SB, Jang SY, Kang HT, Wei B, Jeoun UW, Yoon GS, et al. Modulation of mitochondrial membrane potential and ROS generation by nicotinamide in a manner independent of SIRT1 and mitophagy. *Mol Cells*. 2017;40:503–14.
35. Pickrell AM, Youle RJ. The roles of PINK1, parkin, and mitochondrial fidelity in Parkinson's disease. *Neuron*. 2015;85:257–73.
36. Narendra D, Tanaka A, Suen DF, Youle RJ. Parkin is recruited selectively to impaired mitochondria and promotes their autophagy. *J Cell Biol*. 2008;183:795–803.
37. Rakovic A, Shurkewitsch K, Seibler P, Grünewald A, Zanon A, Hagenah J, et al. Phosphatase and tensin homolog (PTEN)-induced putative kinase 1 (PINK1)-dependent ubiquitination of endogenous Parkin attenuates mitophagy: study in human primary fibroblasts and induced pluripotent stem cell-derived neurons. *J Biol Chem*. 2013;288:2223–37.
38. Gao F, Yang J, Wang D, Li C, Fu Y, Wang H, et al. Mitophagy in Parkinson's disease: pathogenic and therapeutic implications. *Front Neurol*. 2017;8:527.
39. Kumar R, Reichert AS. Common principles and specific mechanisms of mitophagy from yeast to humans. *Int J Mol Sci*. 2021;22:4363.
40. Di Rita A, Peschiaroli AD, Acunzo P, Strobbe D, Hu Z, et al. HUWE1 E3 ligase promotes PINK1/PARKIN-independent mitophagy by regulating AMBRA1 activation via IKKa. *Nat Commun*. 2018;9:3755.
41. Puri R, Cheng XT, Lin MY, Huang N, Sheng ZH. Mul1 restrains Parkin-mediated mitophagy in mature neurons by maintaining ER-mitochondrial contacts. *Nat Commun*. 2019;10:3645.
42. Zheng J, Chen X, Liu Q, Zhong G, Zhuang M. Ubiquitin ligase MARCH5 localizes to peroxisomes to regulate pexophagy. *J Cell Biol*. 2022;221:e202103156.
43. Cunningham CN, Baughman JM, Phu L, Tea JS, Yu C, Coons M, et al. USP30 and parkin homeostatically regulate atypical ubiquitin chains on mitochondria. *Nat Cell Biol*. 2015;17:160–9.
44. Marcassa E, Kallinos A, Jardine J, Rusilowicz-Jones EV, Martinez A, Kuehl S, et al. Dual role of USP30 in controlling basal pexophagy and mitophagy. *EMBO Rep*. 2018;19:e45595.
45. Pickrell AM, Huang CH, Kennedy SR, Ordureau A, Sideris DP, Hoekstra JG, et al. Endogenous Parkin preserves dopaminergic substantia nigral neurons following mitochondrial DNA mutagenic stress. *Neuron*. 2015;87:371–81.
46. Watzlawik JO, Hou X, Fricova D, Ramnarine C, Barodia SK, Gendron TF, et al. Sensitive ELISA-based detection method for the mitophagy marker p-S65-Ub in human cells, autopsy brain, and blood samples. *Autophagy*. 2021;17:2613–28.
47. Rusilowicz-Jones EV, Barone FG, Lopes FM, Stephen E, Mortiboys H, Urbé S, et al. Benchmarking a highly selective USP30 inhibitor for enhancement of mitophagy and pexophagy. *Life Sci Alliance*. 2021;5:e202101287.
48. Cornelissen T, Haddad D, Wauters F, Van Humbeeck C, Mandemakers W, Koentjoro B, et al. The deubiquitinase USP15 antagonizes Parkin-mediated mitochondrial ubiquitination and mitophagy. *Hum Mol Genet*. 2014;23:5227–42.
49. Frank M, Duvezin-Caubet S, Koob S, Occhipinti A, Jagasia R, Petcherski A, et al. Mitophagy is triggered by mild oxidative stress in a mitochondrial fission dependent manner. *Biochim Biophys Acta*. 2012;1823:2297–310.
50. Xiao B, Goh JY, Xiao L, Xian H, Lim KL, Liou YC. Reactive oxygen species trigger Parkin/PINK1 pathway-dependent mitophagy by inducing mitochondrial recruitment of Parkin. *J Biol Chem*. 2017;292:16697–708.
51. Xiao B, Deng X, Lim GGY, Xie S, Zhou ZD, Lim KL, et al. Superoxide drives progression of Parkin/PINK1-dependent mitophagy following translocation of Parkin to mitochondria. *Cell Death Dis*. 2017;8:e3097.
52. French ME, Koehler CF, Hunter T. Emerging functions of branched ubiquitin chains. *Cell Discov*. 2021;7:6.

## ACKNOWLEDGEMENTS

The authors would like to thank Dorte Lyholmer and Nadine Becker-von Buch for excellent technical assistance, Dr. Tore B. Stage for providing access to bioimaging equipment, and Dr. Claire Gudex for editing the manuscript. The live imaging experiments reported in this paper were performed at DaMBIC, a bioimaging research core facility at the University of Southern Denmark. DaMBIC was established by an equipment grant from the Danish Agency for Science Technology and Innovation and by internal funding from the University of Southern Denmark. The research leading to these results was supported by H. Lundbeck A/S, the Innovation Fund Denmark (BrainStem & NeuroStem), the Danish Parkinson Foundation, the Jascha Foundation, the A.P. Møller Foundation for the Advancement of Medical Science (15-396, 14-427), and the Faculty of Health Sciences at the University of Southern Denmark.

## AUTHOR CONTRIBUTIONS

JO, TCS, MA, KF, and MM designed research; JO, JBA, TCS, and HH performed experiments; KF and KKF contributed new reagents or analytic tools; JO, JBA, and HH analyzed data; JO and MM wrote the manuscript. TCS, MA, KKF, and KF revised the manuscript for content. All authors read and approved the final manuscript.

## COMPETING INTERESTS

TCS, MA, and KF work for the pharmaceutical company H. Lundbeck A/S.

## ETHICS APPROVAL AND CONSENT TO PARTICIPATE

The Research Ethics Committee of the Region of Southern Denmark approved the study prior to initiation (S-20130101). All use of human stem cells was performed in accordance with the Danish national regulations and the ethical guidelines issued by the Network of European CNS Transplantation and Restoration (NECTAR) and the International Society for Stem Cell Research (ISSCR).

**ADDITIONAL INFORMATION**

**Supplementary information** The online version contains supplementary material available at <https://doi.org/10.1038/s41419-024-06439-6>.

**Correspondence** and requests for materials should be addressed to Morten Meyer.

**Reprints and permission information** is available at <http://www.nature.com/reprints>

**Publisher's note** Springer Nature remains neutral with regard to jurisdictional claims in published maps and institutional affiliations.



**Open Access** This article is licensed under a Creative Commons Attribution 4.0 International License, which permits use, sharing, adaptation, distribution and reproduction in any medium or format, as long as you give appropriate credit to the original author(s) and the source, provide a link to the Creative Commons license, and indicate if changes were made. The images or other third party material in this article are included in the article's Creative Commons license, unless indicated otherwise in a credit line to the material. If material is not included in the article's Creative Commons license and your intended use is not permitted by statutory regulation or exceeds the permitted use, you will need to obtain permission directly from the copyright holder. To view a copy of this license, visit <http://creativecommons.org/licenses/by/4.0/>.

© The Author(s) 2024